Measurement of Muon Capture on the Proton to 1% Precision and Determination of the Pseudoscalar Coupling g_{P}

V. A. Andreev *et al.* (MuCap Collaboration)

Measurement of Muon Capture on the Proton to 1% Precision and Determination of the Pseudoscalar Coupling g_P

V.A. Andreev,[1] T.I. Banks,[2] R.M. Carey,[3] T.A. Case,[2] S.M. Clayton,[4] K.M. Crowe*,[2] J. Deutsch*,[5] J. Egger,[6] S.J. Freedman*,[2] V.A. Ganzha,[1] T. Gorringe,[7] F.E. Gray,[8,2] D.W. Hertzog,[4,9] M. Hildebrandt,[6] P. Kammel,[4,9] B. Kiburg,[4,9] S. Knaack,[4] P.A. Kravtsov,[1] A.G. Krivshich,[1] B. Lauss,[6] K.R. Lynch,[3] E.M. Maev,[1] O.E. Maev,[1] F. Mulhauser,[4,6] C. Petitjean,[6] G.E. Petrov,[1] R. Prieels,[5] G.N. Schapkin,[1] G.G. Semenchuk,[1] M.A. Soroka,[1] V. Tishchenko,[7] A.A. Vasilyev,[1] A.A. Vorobyov,[1] M.E. Vznuzdaev,[1] and P. Winter[4,9]

(MuCap Collaboration)

[1]*Petersburg Nuclear Physics Institute, Gatchina 188350, Russia*
[2]*Department of Physics, University of California, Berkeley, and LBNL, Berkeley, CA 94720, USA*
[3]*Department of Physics, Boston University, Boston, MA 02215, USA*
[4]*Department of Physics, University of Illinois at Urbana-Champaign, Urbana, IL 61801, USA*
[5]*Institute of Nuclear Physics, Université Catholique de Louvain, B-1348, Louvain-la-Neuve, Belgium*
[6]*Paul Scherrer Institute, CH-5232 Villigen PSI, Switzerland*
[7]*Department of Physics and Astronomy, University of Kentucky, Lexington, KY 40506, USA*
[8]*Department of Physics and Computational Science, Regis University, Denver, CO 80221, USA*
[9]*Department of Physics, University of Washington, Seattle, WA 98195, USA*

The MuCap experiment at the Paul Scherrer Institute has measured the rate Λ_S of muon capture from the singlet state of the muonic hydrogen atom to a precision of 1%. A muon beam was stopped in a time projection chamber filled with 10-bar, ultra-pure hydrogen gas. Cylindrical wire chambers and a segmented scintillator barrel detected electrons from muon decay. Λ_S is determined from the difference between the μ^- disappearance rate in hydrogen and the free muon decay rate. The result is based on the analysis of 1.2×10^{10} μ^- decays, from which we extract the capture rate $\Lambda_S = (714.9 \pm 5.4_{\text{stat}} \pm 5.1_{\text{syst}})$ s^{-1} and derive the proton's pseudoscalar coupling $g_P(q_0^2 = -0.88\,m_\mu^2) = 8.06 \pm 0.55$.

PACS numbers: 23.40.-s, 24.80.+y, 13.60.-r, 14.20.Dh, 11.40.Ha, 29.40.Gx

We report a measurement of the rate Λ_S of ordinary muon capture (OMC),

$$\mu^- + p \to n + \nu_\mu, \tag{1}$$

from the singlet state of the muonic hydrogen atom. The analysis uses the complete dataset of the MuCap experiment, with significantly smaller systematic and statistical uncertainties compared to our earlier publication [1].

For the low momentum transfer $q_0^2 = -0.88 m_\mu^2$ in process (1), the Standard Model electroweak interaction reduces to an effective Fermi interaction between the leptonic and hadronic weak currents. While the leptonic current has a simple $\gamma_\mu(1 - \gamma_5)$ structure, the hadronic current between nucleon states is modified by QCD, as expressed in a model-independent way by the introduction of form factors. Since second-class currents are suppressed, muon capture on the proton involves $g_V(q_0^2)$ and $g_M(q_0^2)$, the vector and magnetic form factors in the vector current, as well as $g_A(q_0^2)$ and $g_P(q_0^2)$, the axial and pseudoscalar form factors in the axial current [2–4]. The first three are well known and contribute only around 0.4% uncertainty to the determination of Λ_S [5]. Our

measurement of Λ_S determines $g_P \equiv g_P(q_0^2)$, the least well known of these form factors.

The pseudoscalar term in the axial nucleon current has played a significant role in the understanding of weak and strong interactions. Initial estimates were based on the concept of a partially conserved axial current, followed by the recognition of its deeper significance as a consequence of chiral symmetry and its spontaneous and explicit breaking [6]. These ideas were foundations for explaining the generation of hadronic masses and the development of chiral perturbation theory (ChPT), the effective field theory of low-energy QCD. Based on well-known low-energy constants,

$$g_P^{\text{Theory}} = 8.26 \pm 0.23 \tag{2}$$

was derived within ChPT [2, 7], with good convergence to two-loop order [8]. Though lattice QCD has advanced to unquenched calculations of g_A and g_P [9, 10], the precision of the ChPT prediction in Eqn. 2 remains unmatched and stands to be tested experimentally.

Muon capture on hydrogen is the most direct means to determine g_P. Such experiments are complicated by the fact that negative muons stopped in hydrogen form not only μp atoms, but subsequently $pp\mu$ molecules where the capture rate differs significantly. Prior to MuCap, the most precise capture rate was measured in liquid hydrogen (LH$_2$) [11], where $pp\mu$ forms rapidly. The value
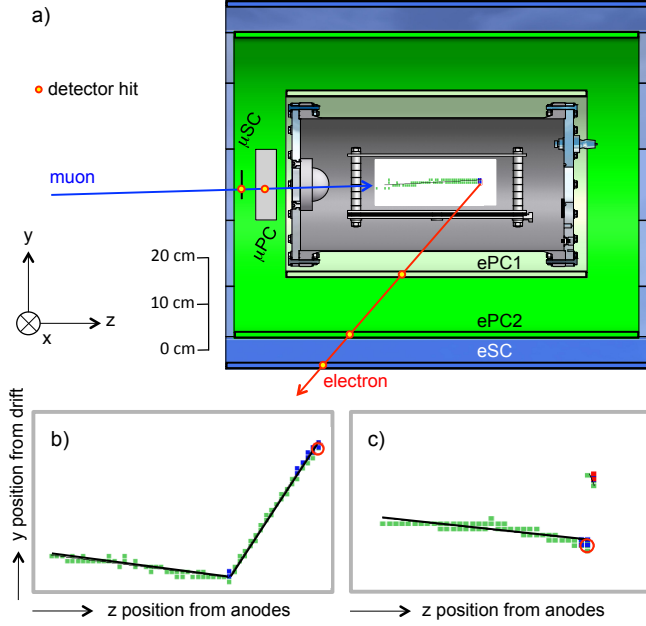
---

*Deceased

FIG. 1: (color online) Upper panel: (a) Cross-sectional view of the MuCap detector showing a typical muon stop and decay electron. Lower panels: zoomed-in special event topologies. (b) Rare large-angle $\mu-p$ scatter event with $\sim 10^{-2}/\mu$ probability. c) Very rare delayed capture on impurity in $\mu O \to N^*\nu$ with $\sim 3.4 \times 10^{-6}/\mu$ probability. The interpretation of the event displays is described in the text.

of g_P extracted under these conditions depends critically on the poorly known ortho-to-para $pp\mu$ transition rate, λ_{op} [12, 13]. The related, rare radiative muon capture (RMC) process $\mu^- p \to n\nu\gamma$ is less sensitive to λ_{op}, but the first experimental result on g_P [14] disagreed with theory. For a discussion of this puzzling situation and muonic processes in hydrogen, see [2–4].

The MuCap experiment was designed to significantly reduce the density-dependent formation of $pp\mu$ molecules by employing a gas density of $\phi \approx 0.01$ (relative to LH$_2$). In these conditions about 97% of the muon captures occur in the μp singlet state. The experimental concept is sketched in Figure 1a. A 34 MeV/c muon beam was stopped in a time projection chamber (TPC) filled with 10-bar, ultra-pure hydrogen gas [15]. The TPC was used to discriminate between muons that stop in the gas and those that reach wall materials, where capture proceeds much faster than in hydrogen. Arriving muons were detected by an entrance scintillator (μSC) and a proportional chamber (μPC), and tracked in the TPC. Outgoing decay electrons were detected by concentric multiwire proportional chambers (ePC1 and ePC2) and a segmented scintillator barrel (eSC). The decay times were histogrammed and fit to an exponential. The difference between the observed disappearance rate λ_{μ^-} and the free muon decay rate λ_{μ^+} [16] is attributed to muon capture, $\Lambda_S \approx \lambda_{\mu^-} - \lambda_{\mu^+}$.

The new data reported here were collected during the 2006 (R06) and 2007 (R07) running periods in the πE3 muon channel at the Paul Scherrer Institute. Properties of the new datasets are compared to our published result (R04) [1] in Table I. Besides the 1.2×10^{10} muon-electron pairs from μ^- stops in hydrogen, additional systematic data included 0.6×10^{10} μ^+ decays and μ^- data collected when the target gas was doped with elemental impurities (nitrogen, water and argon).

TABLE I: Main features of MuCap production runs. Statistics of fully reconstructed $\mu-e$ pairs, deuterium concentration c_D, water concentration c_{H_2O} determined by humidity sensor (not present in R04), and observed impurity capture yield per muon, Y_Z.

quantity	R04	R06	R07
Statistics	1.6×10^9	5.5×10^9	5.0×10^9
c_D (ppb)	1440	<60	<10
c_{H_2O} (ppb)	n/a	18.	8.7
Y_Z (ppm)	12	6.3	3.4

Although the experimental methodology closely followed that of our first result, several hardware upgrades implemented between R04 and R06 led to significantly enhanced performance. In R06 the TPC was operated with about 2.5 times higher gas gain than in R07. As this affects critical chamber parameters, the comparison of the two runs provides an invaluable consistency check.

Events with multiple muons in the TPC (pileup) need to be rejected as they distort the extracted disappearance rate. The maximum rate of the DC muon beam employed in R04 was throttled to minimize pileup. In R06 and R07, the loss of events to pileup was largely eliminated by the introduction of a 25-kV, fast-switching electrostatic kicker [17]. The detection of a muon traversing the μSC triggered the kicker, which deflected the beam for a period of 25.6 μs. The beam extinction factor was around 100 and the rate of pileup-free data was three times larger in R06/7 than in R04.

Another essential change was the greatly improved isotopic and chemical purity of the TPC gas. When deuterium is present (concentration c_D), muons can form μd atoms, which, due to a Ramsauer-Townsend minimum in the scattering cross section [4], can diffuse out of the fiducial volume and distort the disappearance rate. To separate the hydrogen into its isotopic components, a new cryogenic distillation column was installed. Periodic gas samples were analyzed externally using atomic mass spectrometry [18]. For the limits on c_D listed in Table I, transfer to μd leads to distortions of less than 0.74 s^{-1} and 0.12 s^{-1} for the R06 and R07 run periods, respectively. A higher sensitivity of the atomic mass spectrometer was responsible for the improved limit in R07.

In the presence of $Z > 1$ impurities, muons preferentially transfer from μp to μZ atoms, distorting the

disappearance rate. Extended baking of the TPC and increased flux and filtering in the continuous gas purification system [19] led to a fourfold reduced impurity level compared to R04. Moreover, the installation of a humidity sensor before R06 allowed monitoring of the dominant chemical impurity.

Our novel hydrogen TPC was key to the experiment. In the sensitive volume of $x \times y \times z = 15 \times 12 \times 28$ cm^3 with an applied field of 2 kV/cm, ionization electrons from stopping muons drifted down towards the readout plane with a velocity $v_y = -5.5$ mm/μs. They were amplified in a multi-wire proportional chamber region with 72 anodes perpendicular and 36 strip wires parallel to the beam. Anode and cathode signals were discriminated with three energy thresholds and read out by TDCs in 200 ns time intervals. The event display in the center of Figure 1a shows the y-z projection of a typical muon stop in the TPC. The threshold $E_1 \approx 15$ keV is indicated by green pixels. Blue pixels denote the threshold $E_2 \approx 55$ keV, which was set just below the muon's Bragg peak. The threshold $E_3 \approx 315$ keV (red pixels in Figure 1c) was set to record nuclear recoils from muon captures on impurities. In addition to the primary TDC-based readout of the TPC, new 12-bit, 25 MHz flash analog-to-digital converters recorded selectively triggered events.

About 30 TB of raw data was processed at the NCSA supercomputing facility in a multi-stage procedure. Muon stop candidates were constructed from the μSC time and TPC track information. Muon pileup events, flagged by the entrance counters, were rejected. Because the combined inefficiency of the entrance counters was less than 10^{-4}, the residual pileup distorted the observed muon disappearance rate λ_{μ^-} by less than $0.5\,\mathrm{s}^{-1}$. Contiguous pixel regions in the TPC were then fit to a straight line, as indicated by the black line along the muon trajectory in Fig. 1a. In the case of large angle scattering (Fig. 1b) a two-line fit was applied. The muon stop location (red circle) was identified as the most downstream E_2 pixel. The muon track requirements were optimized so as to minimize possible distortions to λ_{μ^-} while suppressing events where the muon could have left the hydrogen gas. Muons that stopped within a fiducial volume $\Delta x \times \Delta y \times \Delta z = 10.4 \times 8.0 \times 20.4\,\mathrm{cm}^3$ were accepted. The minimum track length was 3.2 cm, and the maximum fit χ^2 was 2. λ_{μ^-} was stable against variation of the track length and χ^2 cuts. However, variations in the fiducial volume boundaries produced statistically disallowed deviations, for which a systematic uncertainty of $3.0\,\mathrm{s}^{-1}$ was assigned.

Electron tracks were constructed from coincidences between an eSC segment (comprising four photomultiplier tubes) and hits in the two ePCs (each requiring an anode and at least one cathode plane). In the R06 and R07 run periods, the time and gain stabilities of the eSC were verified by recording their signals in 8-bit, 450 MHz waveform digitizers. While the TPC gain was insufficient

to produce electron tracks with contiguous pixels, a virtual track in the TPC was reconstructed from hits in the eSC and ePCs, as indicated by the red line in Figure 1a. A cut of $b \leq 120$ mm was placed on the impact parameter b between muon stop and electron vector. This loose cut significantly reduces backgrounds (c.f. Fig. 3 in [1]) while minimizing distortions of λ_{μ^-} introduced by a time-dependent acceptance due to μp diffusion. Although μp atoms diffuse only at the mm scale, changes in λ_{μ^-} vs. b were observed. This behavior fixed the single parameter of a μp diffusion model in good agreement with theory [20]. For the applied cut, the model was used to determine small corrections $(-3.1 \pm 0.1)\,\mathrm{s}^{-1}$ and $(-3.0 \pm 0.1)\,\mathrm{s}^{-1}$ for R06 and R07, respectively. To check that λ_{μ^-} was insensitive to the electron track definition, we also constructed coincidences requiring different combinations of anode and cathode planes within the ePCs. This revealed slightly non-statistical variations in λ_{μ^-}, which were fully covered by a $1.8\,\mathrm{s}^{-1}$ systematic uncertainty.

In extreme cases of example Fig. 1b, muons scatter through large angles, leave the TPC volume, and stop on surrounding materials. Because of the lower TPC gain during R07, there were often gaps in the tracks of scattered muons, making it difficult to reliably identify these events. Moreover, the recoil proton could deposit enough energy in the TPC to trigger the E_2 threshold, mimicking an acceptable muon stop. However, these events were unlikely to deposit enough energy at the scattering vertex to exceed the E_2-threshold on neighboring anodes. In the analysis of the R06 and R07 datasets, we required at least two consecutive E_2 anodes at the end of the muon track.

This cut introduced a subtle systematic effect. Electrons that traversed the muon's drifting ionization charge occasionally deposited enough additional energy to elevate a muon's E_1 signal above the E_2 threshold. In rare instances a muon stop with a single E_2 anode was promoted to a stop with two neighboring E_2 anodes. Such events would pass the $\mu - p$ scatter cut described above with a decay-time-dependent acceptance and therefore distort the extracted disappearance rate. Because positive muons are sensitive to the charge interference effect but do not capture on nuclei, we were able to measure the induced distortion [21]. The method was supplemented by neutron data collected in 8 large liquid scintillator detectors: muons scattered into $Z > 1$ materials were found to yield copious neutrons from nuclear capture. The resulting corrections were $(-12.4 \pm 3.22)\,\mathrm{s}^{-1}$ and $(-7.2 \pm 1.25)\,\mathrm{s}^{-1}$ for R06 and R07, respectively. The correction was sensitive to the E_2 threshold, which we decreased in R07, suppressing the interference effect.

As illustrated in Fig. 1c, nuclear capture on impurities was identified by the presence of an E_3 threshold signal in the TPC. This allowed continuous in-$situ$ monitoring of the yield Y_Z of these events. The average val-

ues for Y_Z over the three datasets are given in Table I and track well with the humidity sensor readings. To calibrate the necessary correction, special runs were conducted in which the hydrogen gas was doped with known amounts of nitrogen or water vapor. The changes in the disappearance rate and Y_Z were measured relative to the pure, undoped hydrogen data. Scaling by the observed Y_Z then determined the corrections for residual impurities: $(-7.80 \pm 1.87)\,\mathrm{s}^{-1}$ and $(-4.54 \pm 0.93)\,\mathrm{s}^{-1}$ in R06 and R07, respectively.

To obtain the final muon disappearance rate, the muon stops and electron tracks were first sorted into muon-electron pairs. The decay time, $t \equiv t_{\mathrm{eSC}} - t_{\mu\mathrm{SC}}$, was histogrammed and fit with the function $N(t) = N_0 \cdot w \cdot \lambda_{\mu^-} \cdot e^{-\lambda_{\mu^-} t} + B$ over the range $160\ \mathrm{ns} < t < 19000\ \mathrm{ns}$. The bin width w was fixed at 80 ns, while N_0, B and λ_{μ^-} were free parameters. To avoid analysis bias, the exact clock frequency was hidden from the analyzers. After it was revealed, we obtained

$$\lambda_{\mu^-}(\mathrm{R06}) = 455857.3 \pm 7.7_{\mathrm{stat}} \pm 5.1_{\mathrm{syst}}\ \mathrm{s}^{-1}, \quad (3)$$

$$\lambda_{\mu^-}(\mathrm{R07}) = 455853.1 \pm 8.3_{\mathrm{stat}} \pm 3.9_{\mathrm{syst}}\ \mathrm{s}^{-1}. \quad (4)$$

Because the fit $\chi^2/\mathrm{DOF} = 1.2 \pm 0.1$ was slightly larger than expected for both R06 and R07, these values reflect inflated statistical uncertainties following the S-factor prescription [5]. The 3-parameter fitting procedure was complemented by applying a full kinetics fit which included all atomic- and molecular-state effects as well as water and nitrogen impurities; the result was consistent within $0.2\,\mathrm{s}^{-1}$.

In order to check the consistency of our result, we examined changes in λ_{μ^-} with respect to variations in data selection. The fit start and stop times were varied over a range of several microseconds and the parameters remained stable. Only statistical variations were observed when the data was sorted chronologically by run number. Since many of the subtle couplings between the muon and electron definitions are geometrical, the observed stability of the result with respect to azimuth was a critical cross-check.

Table II summarizes the aforementioned corrections to our λ_{μ^-} result as well as the systematic uncertainties. Two additional corrections are required to correctly express λ_{μ^-} as:

$$\lambda_{\mu^-} = \left(\lambda_{\mu^+} + \Delta\lambda_{\mu p}\right) + \Lambda_S + \Delta\Lambda_{pp\mu}. \quad (5)$$

Here $\Delta\lambda_{\mu p}$ is a calculable μp bound-state effect [22, 23], while $\Delta\Lambda_{pp\mu}$ accounts for the around 3% of muons that capture from molecular states. The latter depends on λ_{op} and $\lambda_{pp\mu}$ and is derived from fits to simulated data generated with the precise experimental conditions (gas density $\phi = 0.0115 \pm 0.0001$, background level, impurity concentrations, and fit ranges). We used $\lambda_{op} = (6.6 \pm 3.4) \times 10^4$ [4] and a newly determined value of $\lambda_{pp\mu} = (1.94 \pm 0.06) \times 10^6\,\mathrm{s}^{-1}$ [24], which was measured

TABLE II: Applied corrections and systematic errors.

Effect	Corrections and uncertainties [s^{-1}]	
	R06	R07
$Z > 1$ impurities	-7.8 ± 1.87	-4.54 ± 0.93
$\mu - p$ scatter removal	-12.4 ± 3.22	-7.2 ± 1.25
μp diffusion	-3.1 ± 0.10	-3.0 ± 0.10
μd diffusion	± 0.74	± 0.12
Fiducial volume cut	± 3.00	± 3.00
Entrance counter ineff.	± 0.50	± 0.50
Electron track def.	± 1.80	± 1.80
Total λ_{μ^-} corr.	-23.30 ± 5.20	-14.74 ± 3.88
μp bound state: $\Delta\lambda_{\mu p}$	-12.3 ± 0.00	-12.3 ± 0.00
$pp\mu$ states: $\Delta\Lambda_{pp\mu}$	-17.73 ± 1.87	-17.72 ± 1.87

by admixing 19.6 ± 1.1 ppm of argon to the TPC's hydrogen. It agrees with the previous world average [4] but is three times more precise. Evaluating Eqn. 5 and including the updated positive muon decay rate of 455170.05 ± 0.46 s^{-1} [5, 16], we determine the singlet capture rates:

$$\Lambda_S(\mathrm{R06}) = 717.3 \pm 7.73_{\mathrm{stat}} \pm 5.55_{\mathrm{syst}}\ \mathrm{s}^{-1}, \quad (6)$$

$$\Lambda_S(\mathrm{R07}) = 713.1 \pm 8.33_{\mathrm{stat}} \pm 4.34_{\mathrm{syst}}\ \mathrm{s}^{-1}. \quad (7)$$

We also update slightly our previous publication [1] using the latest values for λ_{μ^+}, λ_{op}, and $\lambda_{pp\mu}$, to obtain $\Lambda_S(\mathrm{R04}) = 713.5 \pm 12.5_{\mathrm{stat}} \pm 8.6_{\mathrm{syst}}\ \mathrm{s}^{-1}$. Accounting for correlated systematics among these three datasets, we report a final, combined result

$$\Lambda_S^{\mathrm{MuCap}} = 714.9 \pm 5.4_{\mathrm{stat}} \pm 5.1_{\mathrm{syst}}\ \mathrm{s}^{-1}. \quad (8)$$

This new result is in excellent agreement with recent theory [25–27]. From the latest calculation [27], we derive

$$\Lambda_S^{\mathrm{Th}}(g_A, g_P) = (712.7 \pm 3.0 \pm 3.0)\times$$
$$\left[1 + 0.6265(g_A - g_A^{\mathrm{PDG}}) - 0.0108(g_P - g_P^{\mathrm{Th}})\right]^2\ \mathrm{s}^{-1}, \quad (9)$$

where all form factors are evaluated at q_0^2. Eqn. 9 quantifies the dependence of the theoretical capture rate on the choice of g_P, relative to value $g_P^{\mathrm{Th}} = 8.2$ used in Ref. [27], and on g_A, relative to the latest $g_A^{\mathrm{PDG}}(0) = 1.2701 \pm 0.0025$ [5]. The two uncertainties in the equation stem from limited knowledge of g_A and radiative corrections. Setting $\Lambda_S^{\mathrm{Th}}(g_A^{\mathrm{PDG}}, g_P^{\mathrm{MuCap}})$ to $\Lambda_S^{\mathrm{MuCap}}$ gives

$$g_P^{\mathrm{MuCap}}(q_0^2 = -0.88\,m_\mu^2) = 8.06 \pm 0.48 \pm 0.28, \quad (10)$$

where the two uncertainties arise from the error propagation of $\Lambda_S^{\mathrm{MuCap}}$ and Λ_S^{Th}, respectively. If we would have updated $g_A(0)$ to 1.275, as advocated in [28] and supported by recent measurements of the neutron β-decay
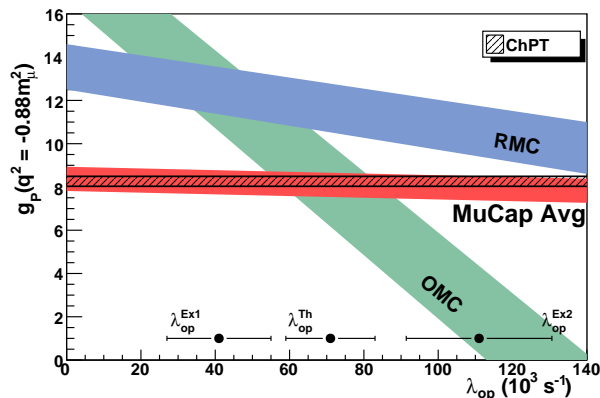
FIG. 2: Extracted values for g_P as a function of the poorly known molecular transition rate λ_{op} [12, 13, 31]. In contrast to earlier experiments (OMC [11], RMC [14]), MuCap is rather insensitive to this parameter.

asymmetry [29, 30], the g_P extracted from MuCap would increase to 8.34.

Figure 2 illustrates the excellent agreement with the theoretical prediction, Eqn. 2, and highlights MuCap's reduced sensitivity to the molecular parameter λ_{op}. This answers the longstanding challenge of an unambiguous measurement of g_P, generated by the mutual inconsistency of earlier experiments (OMC, RMC) and their strong sensitivity to λ_{op}. Corroborating values for g_P are obtained in recent analyses [32, 33] of an earlier 0.3% measurement of muon capture on ^{3}He [34], with uncertainties limited by theory. MuCap provides the most precise determination of g_P in the theoretically clean μp atom and verifies a fundamental prediction of low-energy QCD.

[1] V. A. Andreev et al. (MuCap Collaboration), Phys. Rev. Lett. **99**, 032002 (2007), arXiv:0704.2072.
[2] V. Bernard, L. Elouadrhiri, and U.-G. Meissner, J. Phys. **G28**, R1 (2002).
[3] T. Gorringe and H. W. Fearing, Rev. Mod. Phys. **76**, 31 (2004).
[4] P. Kammel and K. Kubodera, Annual Review of Nuclear and Particle Science **60**, 327 (2010).
[5] J. Beringer et al. (Particle Data Group), Phys. Rev. **D86**, 010001 (2012).
[6] Y. Nambu, Phys. Rev. Lett. **4**, 380 (1960).
[7] V. Bernard, N. Kaiser, and U.-G. Meissner, Phys. Rev. **D50**, 6899 (1994).
[8] N. Kaiser, Phys. Rev. **C67**, 027002 (2003).
[9] T. Yamazaki et al. (RBC and UKQCD Collaborations), Phys. Rev. **D79**, 114505 (2009).
[10] C. Alexandrou et al., Phys. Rev. D **83**, 045010 (2011).
[11] G. Bardin et al., Nucl. Phys. **A352**, 365 (1981).
[12] G. Bardin et al., Phys. Lett. **B104**, 320 (1981).
[13] J. H. D. Clark et al., Phys. Rev. Lett. **96**, 073401 (2006).
[14] D. H. Wright et al., Phys. Rev. **C57**, 373 (1998).
[15] J. Egger, M. Hildebrandt, and C. Petitjean (MuCap Collaboration), Nucl. Instrum. Meth. **A628**, 199 (2011).
[16] D. Webber et al. (MuLan Collaboration), Phys. Rev. Lett. **106**, 041803 (2011).
[17] M. Barnes and G. Wait, IEEE Trans. Plasma Sci. **32**, 1932 (2004).
[18] M. Döbeli et al., Nucl. Instrum. Meth. **B266**, 1820 (2008).
[19] V. Ganzha et al., Nucl. Instrum. Meth. **A578**, 485 (2007).
[20] A. Adamczak, Phys. Rev. **A74**, 042718 (2006).
[21] B. Kiburg, Ph.D. thesis, UIUC (2011).
[22] H. Überall, Phys. Rev. **119**, 365 (1960).
[23] H. Von Baeyer and D. Leiter, Phys. Rev. **A19**, 1371 (1979).
[24] S. Knaack, Ph.D. thesis, UIUC (2012).
[25] V. Bernard, T. R. Hemmert, and U.-G. Meissner, Nucl. Phys. **A686**, 290 (2001).
[26] S. Ando, F. Myhrer, and K. Kubodera, Phys. Rev. **C63**, 015203 (2000).
[27] A. Czarnecki, W. J. Marciano, and A. Sirlin, Phys. Rev. Lett. **99**, 032003 (2007).
[28] E. Blucher and W. Marciano, V_{ud}, V_{us}, The Cabibbo Angle and CKM Unitarity, in J. Beringer et. al (Particle Data Group), Phys. Rev. **D86**, 010001 (2012), 852.
[29] D. Mund, B. Maerkisch, M. Deissenroth, J. Krempel, M. Schumann, et al. (2012), arXiv:1204.0013.
[30] M. Mendenhall et al. (UCNA Collaboration) (2012), arXiv:1210.7048.
[31] D. D. Bakalov, M. P. Faifman, L. I. Ponomarev, and S. I. Vinitsky, Nucl. Phys. **A384**, 302 (1982).
[32] L. E. Marcucci, A. Kievsky, S. Rosati, R. Schiavilla, and M. Viviani, Phys. Rev. Lett. **108**, 052502 (2012).
[33] D. Gazit, Nucl. Phys. **A827**, 408c (2009).
[34] P. Ackerbauer et al., Phys. Lett. **B417**, 224 (1998).